Non-invasive measurement of journal bearing lubricant viscosity by means of a novel ultrasonic measurement technique

M.M. Schirru [1], R.S. Mills [1], O. Smith [2], R.S. Dwyer-Joyce [1], M. Sutton [2]

[1] The University of Sheffield, Sheffield, UK, [2] The Lubrizol Corp., Wickliffe, USA

Abstract

An ultrasonic viscometer was used to measure the circumferential viscosity variation in a journal bearing non-invasively. This sensing technique is based on the reflection of a shear wave at a solid-liquid boundary that depends on the viscosity of the liquid and the acoustic properties of the solid. Very little ultrasonic energy can propagate into the oil at a metal-oil interface because the acoustic mismatch is significant. Interleaving a matching layer between the metal and the lubricant enables accurate ultrasonic viscosity measurements [1]. This technique has been used to build a miniaturized ultrasonic viscometer that is accommodated inside a journal to obtain the circumferential viscosity profile. Four viscosity regions are identified due to the variations in the localized temperatures and loads. The results are compared with the isoviscous solution of the Reynolds equations for hydrodynamic lubricated bearings. The ultrasonic viscometer locates the angle at which the maximum load occurs and the length of the loaded contact with good accuracy. Finally, the viscosity results are used to estimate the frictional power losses. It is shown that over 70 % of the total losses in the journal bearing occur in the region where the load is maximum.

1. Introduction

Lubricant viscosity is directly linked to the energy losses in a journal bearing. Smart lubricant design aims to minimise the oil viscosity in parts of the bearing that do not support load, while maximizing the viscosity only where high load requires high localized viscosity to guarantee a full lubrication layer. Given this, a method to accurately measure the viscosity is of importance to improve the current design of journal bearings.

Engine oil viscosity is normally measured by steady shear techniques that require the oil to be extracted from the contact. This operation alters the condition at which the oil operates, because common viscometers cannot reproduce the condition of pressure, temperature and contact that are present at the contact of engine components.

This limitation of conventional viscometers can be overcome by vibrational viscometers operating with piezoelectric transducers. These sensors have the potential to be miniaturized to fit the complex geometry of an engine and to study the lubricant in the contacts. Mason [2] was the first to correlate the reflected energy from a piezoelectric (PZT) quartz crystal to the viscosity of a liquid sample in contact with the transducer. Mason's principle was used in industry to develop different viscometers for general fluid analysis [3, 4, 5]. Lubricating oils were studied for the first time by Barlow and Lamb [6, 7]. The aim of these researchers was to use the novel ultrasonic method to measure oil films non-invasively and to obtain data to validate the findings of Dowson [8] in the elastohydrodynamic lubrication (EHL) field. They developed analytical models for the analysis of non-linear fluid behaviour that considered the effect of the lubricant relaxation time. The solution

was too complex for an actual in-situ setup. Recently, an empirical model based on a simplified Maxwell model algorithm was developed to measure lubricating oils viscosity in-situ in engines [9].

In spite of the improvements in ultrasonic techniques, direct viscosity measurement in components such as engine bearings has not previously been possible. Most engine bearing materials are metallic and so are highly acoustically mismatched with the lubricant. This means that very little of the ultrasonic wave propagates into the liquid and measurements of reflection are subject to significant scatter [9].

The sensitivity of the reflectance technique is enhanced by interleaving a matching layer between the oil and the solid component. The use of a matching layer to improve the sensitivity of ultrasonic measurements dates back to the early 1950s [] when the first immersion longitudinal transducers were designed, but it found little use in shear wave sensors design [11]. In this work the matching layer approach is used to enhance the sensitivity of ultrasonic shear viscometry for in-situ measurements in a journal bearing.

2. Principles of the Ultrasonic Matching Layer Viscometer

The theory and operating principles of this ultrasonic viscometer have been described in detail in a previous work [1]. This section focuses, then, on presenting the use of this viscometer and on how to select appropriately the matching layers for automotive applications.

2.1 Acoustic Mismatch and the Matching Layer

Figure (1 a) shows schematically the conventional setup used in ultrasonic reflectance viscometry.

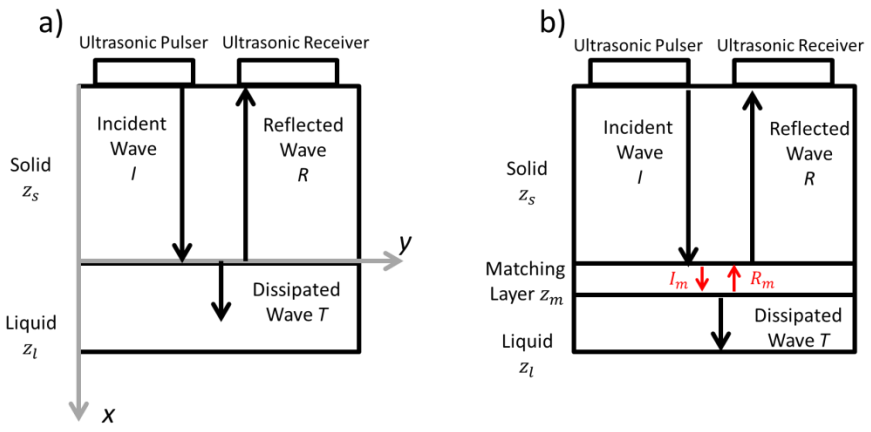

Figure 1: Ultrasonic reflectance viscometry principle. a) Conventional reflectance setup, b) Matching layer method

An ultrasonic polarized shear wave is produced by a piezoelectric transducer and propagates throughout the solid medium. When the ultrasonic wave is incident (*I*) to the interface between the solid and the liquid, the wave energy is partly reflected back (*R*) and partly transmitted in the second medium (*T*). If the second medium is a fluid, the energy of the ultrasonic transmitted wave is quickly dissipated because fluids cannot withstand shear waves for long distances. The magnitude of the energy of the reflected wave, on the other hand, is a function of the mechanical and acoustic properties of the first medium and the viscosity of the fluid. The relation that correlates these quantities is:

$$R = \frac{z_s - z_l}{z_s - z_l} \tag{1}$$

Where z_s is solid acoustic impedance and z_l is the fluid acoustic impedance that is a function of viscosity. The liquid acoustic impedance is defined as:

$$Z_l = [\rho(G' + iG'')]^{\frac{1}{2}} \tag{2}$$

Where ρ is density of the fluid, G' is the shear storage modulus and G'' the shear loss modulus. The ultrasonic reflection coefficient is, then, correlated to the acoustic and viscoelastic properties of the solid-liquid interface. Lubricating oils are, usually, non-Newtonian and an algorithm that reflects the viscoelastic behaviour of these fluids is needed. It is widely accepted that the viscoelastic Maxwell model describes sufficiently well the interaction between an ultrasonic shear wave and a non-Newtonian liquid with a dominant relaxation time at a solid-liquid interface [12, 13, 14]. Figure 2 schematically shows the interaction between a solid particle m_s and a liquid particle m_l at a solid-liquid interface with a spring-dashpot Maxwell model when an oscillatory shear stress is applied.

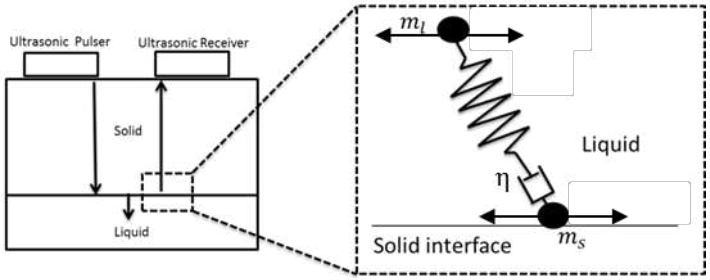

Figure 2: Schematic representation of the Maxwell model

The damper element models the relaxation effects of a viscoelastic system as ultrasonic shear occurs at the solid-liquid boundary, while the spring element is used to model the instantaneous materials deformation. Lamb [6] obtained the viscoelastic properties of a Maxwell liquid under oscillatory shear as:

$$\frac{G'}{G_\infty} = \frac{4\left(\frac{\omega\eta}{2G_\infty}\right)^{\frac{3}{2}}\left[1 + \left(\frac{\omega\eta}{2G_\infty}\right)^{\frac{1}{2}}\right]}{\left\{\left[1 + \left(\frac{\omega\eta}{2G_\infty}\right)^{\frac{1}{2}}\right]^2 + \left(\frac{\omega\eta}{2G_\infty}\right)\right\}^2} \tag{3}$$

$$\frac{G''}{G_\infty} = \frac{2\left(\frac{\omega\eta}{2G_\infty}\right)\left[1 + 2\left(\frac{\omega\eta}{2G_\infty}\right)^{\frac{1}{2}}\right]}{\left\{\left[1 + \left(\frac{\omega\eta}{2G_\infty}\right)^{\frac{1}{2}}\right]^2 + \left(\frac{\omega\eta}{2G_\infty}\right)\right\}^2} \tag{4}$$

Where G_∞ is the infinite shear modulus and G' and G'' are derived from the reflection coefficient by combining equations (1) and (2). G_∞ cannot be measured using the reflectance technique alone, so is not suitable for in-situ measurements. However, it was proven that the Maxwell model can be satisfactory used at limiting shear [12] for which $G_\infty = \frac{\eta}{\tau}$. Under this assumption, the Maxwell model becomes:

$$\eta = \frac{{z_s}^2}{\rho_l \omega}\left(\frac{4|R|(1-|R|^2)sin\theta}{(1+|R|^2+2|R|cos\theta)^2}\right)(1+\omega^2\tau^2) \tag{5}$$

Where τ is measured as [1]:

$$\tau = \sqrt{\left(\frac{\omega\eta}{G''}-1\right)\frac{1}{\omega^2}} \tag{6}$$

In equation (5) the term $\frac{{z_s}^2}{\rho_l \omega}\left(\frac{4|R|(1-|R|^2)sin\theta}{(1+|R|^2+2|R|cos\theta)^2}\right)$ corresponds to the viscosity value for a perfectly Newtonian fluid, while the term $(1+\omega^2\tau^2)$ takes into account of viscoelastic relaxation effects. Equation (5) is particularly useful because it allows a direct correlation between the reflection coefficient R to the viscosity η without relying on any other rheological method.

Equation (5) shows that a correlation exists between the fluid viscosity and the experimentally measurable quantity *R*. However, it is not practically possible to apply this relation to the case study where the solid is a metal and the fluid is a lubricant layer, as shown in Figure (1 a). This is because the shear acoustic impedance of steel is about 25-30 MRayl and the acoustic impedance of oil is less than 1 MRayl. When these values are inserted in equation (1) the reflection coefficient *R* is very close to the unity. This corresponds to the case in which no oil is in contact to the solid because the contribution of z_l to equation (1) is negligible; consequently no practical measurement of the oil properties can be performed. This phenomenon is called acoustic mismatch and is the reason why ultrasonic viscometry could not be applied to the materials typically found in engines. In this work, acoustic mismatch is overcome by insertion of a third layer between solid and liquid, as it is shown in Figure (1 b). This layer is called matching layer because it enables for a better transmission of sound from the solid layer to the fluid, as it is discussed in more detail in the next sections. This method is used in this paper to design an ultrasonic viscometer that is miniaturized and used to measure bearing oil viscosity in-situ.

2.2 Reflection from a three layered system

The theory of the reflection of ultrasonic waves in a three layered system is summarized in this section. Figure (3 a) shows the reflection of an ultrasonic polarized plane shear wave that is normally incident on the interfaces of the three layered system consisting of a solid, matching layer and a liquid.

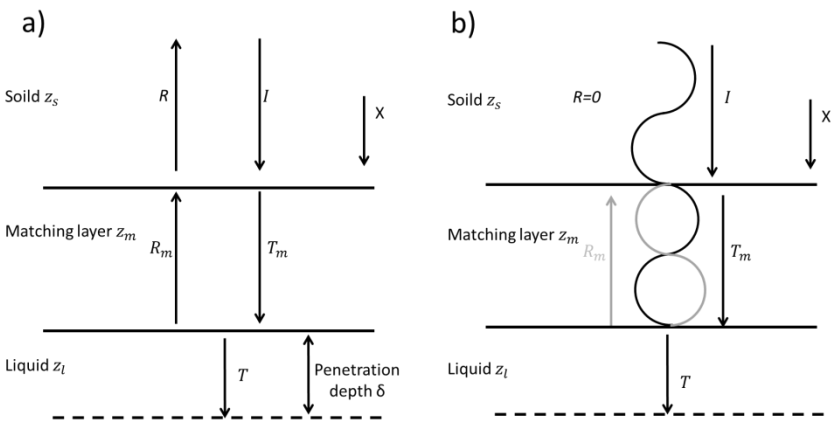

Figure 3: a) Reflection and transmission of a shear wave in the three layered system, b) Resonance at the solid-matching layer interface due to destructive interaction of incident and reflected waves

In Figure (3 a), *I* is the amplitude of the incident wave, *R* is the total ultrasonic energy reflected from the three layered system, R_m is the amplitude of the reflection at the matching layer-liquid boundary, T_m is the amplitude of the energy transmitted at the solid-matching layer boundary, *T* is the total energy transmitted in the fluid and *x* is the shear wave direction of propagation. The total reflection coefficient *R* is calculated as [14]:

$$R = 1 - \frac{2}{\sqrt{\left[2 + \left(\frac{z_l}{z_s} + \frac{z_s}{z_l}\right) cos^2(k_m t) + \left(\frac{{z_m}^2}{z_s z_l} + \frac{z_s z_l}{{z_m}^2}\right) sin^2(k_m t_m)\right]}} \quad (7)$$

Where z_m is the matching layer acoustic impedance, t_m is the matching layer thickness and $k_m = \frac{2\pi}{\lambda_m}$ is the matching layer wave number, and λ_m is the wavelength in the matching layer. The acoustic mismatch between solid and liquid is overcome by exciting resonance between incident and reflected waves from the matching layer. Inside the quarter wavelength matching layer the waves superimpose in phase while, simultaneously, the reflected wave from the matching layer cancels out the incident wave, as shown in Figure (3 b). The total effect is a large increase in the ultrasonic measurement sensitivity because the total reflected energy $R \ll 1$.

2.3 Selection of the Matching Layer

Equation (7) shows that ultrasonic resonance in the three-layered system is dependent upon the thickness and the acoustic impedance of the matching layer. The matching layer thickness is chosen to minimize the reflection coefficient, thus overcoming the previously described limitations. To do so, the matching layer thickness has to be equal to a multiple of a quarter of the wavelength in the layer:

$$t_m = \frac{nc_m}{4f} \quad (8)$$

Where *n* is a natural integer. If equation (8) in inserted in equation (7) then $cos^2(k_m t) = \cos\left(\pi/2\right) = 0$ and $sin^2(k_m t) = \sin\left(\pi/2\right) = 1$ and this leads to the following simplification for equation (7):

$$R = 1 - \sqrt{\frac{4z_s z_l}{\left(z_m + \frac{z_s z_l}{z_m}\right)^2}} \quad (9)$$

Solving equation (9) for minimum reflection (i.e. *R*=0) gives a matching layer acoustic impedance of:

$$z_m = \sqrt{z_s z_l} \quad (10)$$

For a particular case with material properties z_l and z_s and a wave frequency *f*, equation (8) and (10) provide the layer thickness and material that give *R*=0. However, the value of z_m in equation (10) is not constant because z_l varies depending on the density and viscosity of the fluid. For a Newtonian fluid the impedance of the lubricant is approximated as [16]:

$$z_l = \sqrt{\rho_l 2\pi f \eta} \quad (11)$$

Equations (10) and (11) highlight that, given a certain setup solid-matching layer, the reflection coefficient of equation (1) is zero only for a specific fluid. When the fluid viscosity changes, the superposition of the reflected and incident wave is not perfectly resonating, because the magnitude of the waveform reflected from the matching layer-liquid boundary changes. As a consequence, the reflected amplitude is non-zero.

2.4 Effect of the Matching Layer

Figure (4) shows an example plot of equation (7) for two different oils of viscosities of 0.25 Pas and 0.01 Pas when the solid line is aluminium, $z_s = 8\ MRayl$ at the resonance frequency of 5 MHz. The matching layer is designed to match the fluid with viscosity of 0.25 Pas at resonance, so at 5 MHz the reflection coefficient for this oil is equal to zero. For measurement frequencies below and above 5 MHz the reflection coefficient is non-zero. Similarly when the 0.01 Pas oil is considered the reflection coefficient is non-zero at the resonance frequency. Figure (4) shows that at the resonance frequency the two fluids are well discriminated, while outside resonance the fluids are not discriminated. This is because resonance cannot occur outside that specific frequency region, and reflection is less sensitive to the fluid presence. Because of this, particular attention has to be taken in designing the matching layer to operate with the maximum expected oil viscosity.

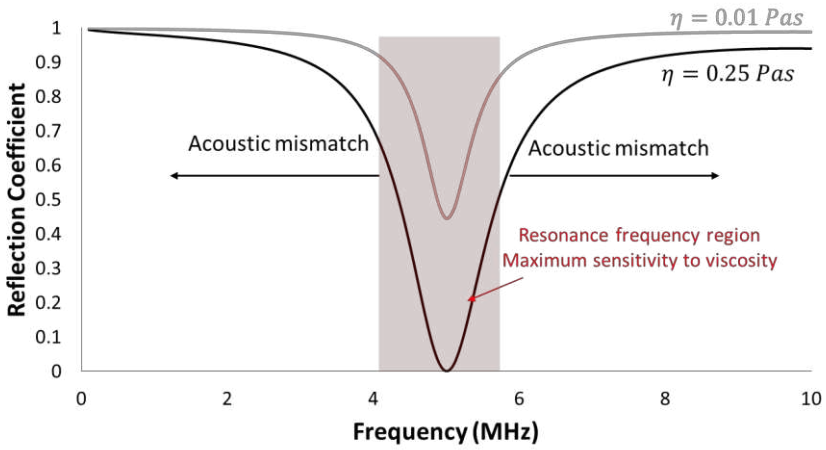

Figure 4: Reflection coefficient sensitivity increment at resonance due to the presence of a matching layer

Apparatus and experimental procedure

3.1 The Matching Layer Ultrasonic Plug

The matching layer method offers the possibility of measuring viscosity at metal-oil interfaces. In this work, a matching layer ultrasonic plug is manufactured and inserted in a journal bearing shaft to measure the oil film viscosity in-situ and real time around the bearing circumference. Figure (5 a) shows schematically the ultrasonic plug and its location in the journal. A pair of 5 MHz piezoelectric PZ5 shear transducers was bonded to the top surface of an aluminium cylindrical plug of 20 mm length and 15 mm of diameter. One transducer is the pulsing element (pulser), while the other receives the reflected ultrasonic wave (receiver). A 50 µm thick polyimide layer was used as matching layer and bonded to the plug surface in contact with the oil. This thickness was calculated using equation (8) and (10) for a resonance frequency of 4.5 MHz. The combination of aluminium and polyimide was found to be ideal for maximizing the measurement sensitivity, while minimizing the measurement noise [1]. The ultrasonic plug was press fitted into the steel journal of the tested journal bearing. The journal has been manufactured from EN24T steel to resemble the geometry of a section of common automotive diesel engines. The length over diameter ratio for this bearing was L/D=0.6. Figure (5 b) shows that half of the shaft was hollow to allow the probe cabling because the ultrasonic viscometer was mounted in the shaft to measure the circumferential viscosity as the shaft was rotated. The shaft was 300 mm long with a journal diameter of 50 mm. The bush was made of brass with internal diameter of 30 mm. The feeding hole consisted of a cylindrical hole that is positioned at the top of the bush. The position of the feeding hole was chosen so that the lubricant was fed where the minor load was present so that full lubricated film could form. The bush and the shaft radius were calculated for maximum radial clearance of 50 µm. This value of clearance was chosen to help the formation of a fully lubricated layer of oil.

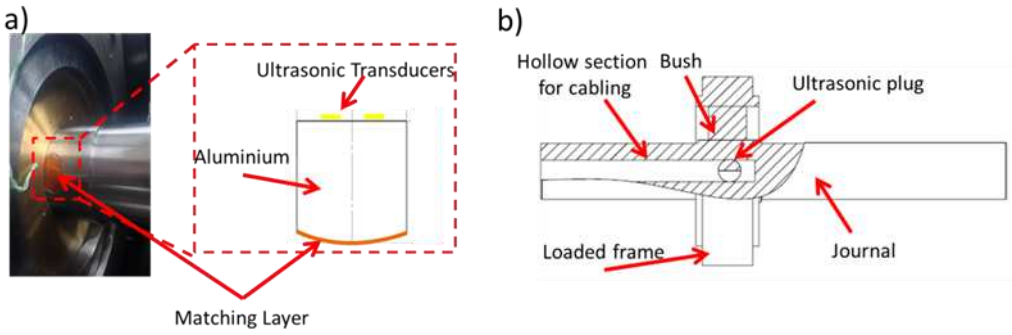

Figure 5: a) Scheme of the ultrasonic plug and its location in the journal b) section of the instrumented journal

3.2 The Journal Bearing Rig

Figure (6) shows the journal bearing rig. The brass bush was contained in a frame that maintained the journal bearing assembly stable when rotating and distributed the load applied. The load was applied to the bearing by a hydraulic ram. For this experiment the applied load varied from 10- 15kN to have a considerable change in viscosity in the maximum loaded region. The ends of the journal were supported by two bearings and the shaft rotation was driven by a pulley connected to an electric motor. The rotational speed of the electric motor was controlled by an inverter. The maximum rotational speed was 1000 rpm. K-type thermocouples measured the temperature at the

journal bearing surface in eight different positions. The thermocouples were located in holes of 1 mm diameter at a depth of 5 mm from the contact surface.

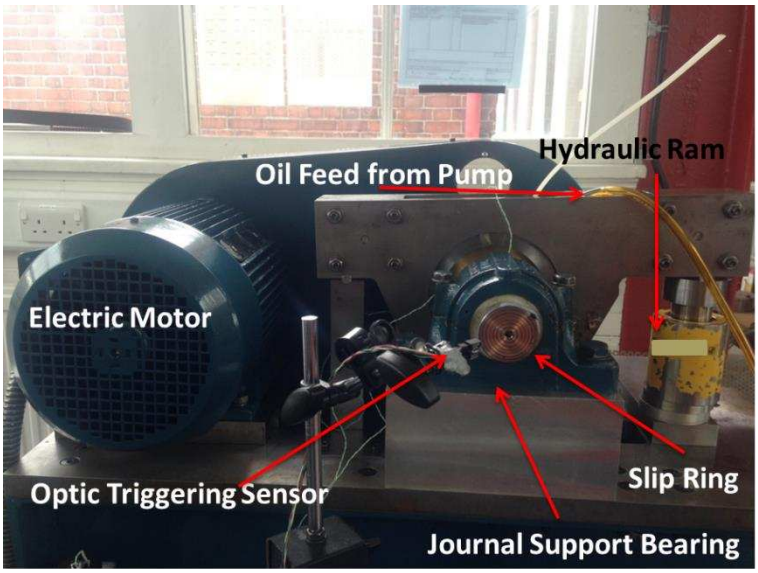

Figure 6: the journal bearing test rig for viscosity measurement

3.3 Instrumentation

Figure (7) schematically shows the experimental instrumentation. There are two waveform generators (type TTI TG5011). The first waveform generator is activated when the optical sensor passes through the trigger point once every revolution of the journal. When the waveform generator 1 is triggered, it sends an impulse signal to the waveform generator 2. This enables data acquisition at fixed pre-defined positions.

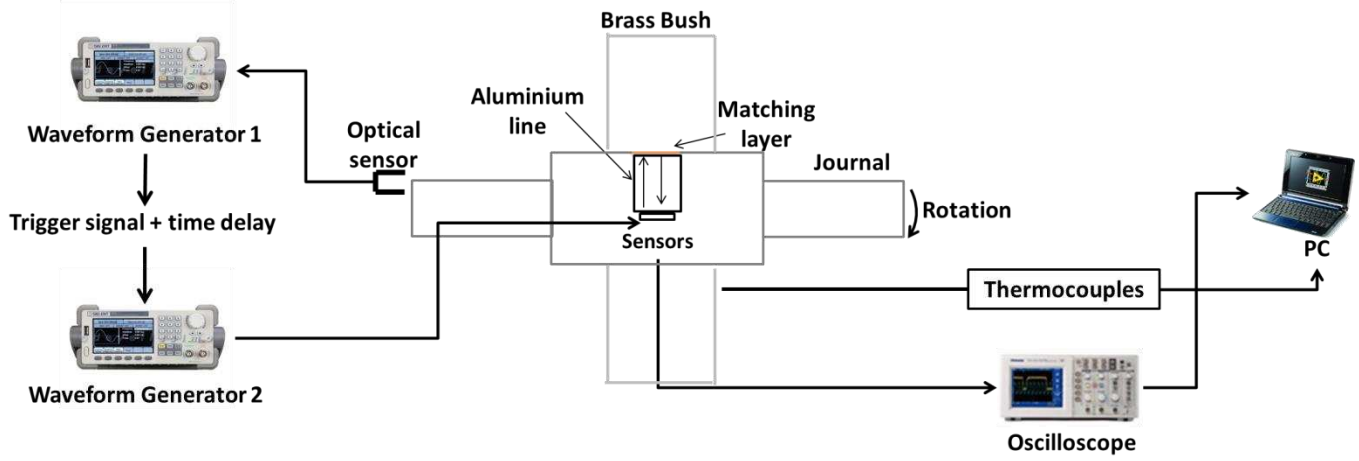

Figure 7: Scheme of the measurement chain of the journal bearing test rig

The acquisition positions were determined by adding a delay to the triggering signal. When the waveform generator 2 was activated it sent a pulsing signal to the emitting transducer. The reflected signal from the journal-oil interface was received by a second transducer (receiver) and displayed on

a Lecroy™ LT342 type oscilloscope. The data were then continuously acquired in a PC where a LabView™ code converted the reflection coefficient to viscosity according to equation (5).

3.4 Test Lubricants

The lubricants chosen were two base oils, an ester and a PAO40, and one fully formulated oil which contains a viscosity modifier (VM). The lubricants were selected for their structure interaction with the ultrasound at high frequencies. Table (1) reports the viscosity data for the test oils. The viscosity was measured with a conventional rheometer (AR G2™ from TA Instruments) at the shear rate of 100 Hz, and with an ultrasonic matching layer ultrasonic viscometer at the frequency of 4.5 MHz. This was an ultrasonic plug with the same characteristic as the one inserted in the journal bearing, but used outside the bearing test rig to characterize the test oils. The Ester sample is a base oil that shows Newtonian behaviour even at high frequencies because the viscosity measured with the ultrasonic viscometer corresponds to the measurement performed with a steady shear cone rheometer. The PAO40 sample is a base oil with a complex molecular structure that make it non-Newtonian. The shear thin of the ultrasonic results in comparison to the steady shear ones is due to the high molecular weight of the PAO40. When the PAO40 is subject to high shear frequencies the molecules tend to pack up thus the overall measured viscosity reduces. Finally, the sample VM shear thins because the polymer cannot relax fast enough at high ultrasonic frequencies. This means that the ultrasonic viscometer measures the viscosity of the base oil for the VM sample. This is of interest for oil manufacturers because knowing how the base oil evolves and degrades in the journal bearing contact can help designing better polymers to interact with that base oil.

	Viscosity (mPas), 20 °C		**Viscosity (mPas), 40 °C**		**Viscosity (mPas), 60 °C**	
Sample	100 Hz	4.5 MHz	100 Hz	4.5 MHz	100 Hz	4.5 MHz
Ester	230	216	99	90	50	45
PAO40	915	450	350	190	158	113
VM	118	32	42	15	31	6

Table 1: Oil samples viscosity measured at different frequencies

Table (1) shows the difference between the viscosity measured with a steady shear and an oscillatory technique. This difference arises because the response of high inertia particles and additives at high ultrasonic frequencies is too slow to completely relax. As a consequence the reflected ultrasonic wave at high ultrasonic frequency is function of the base oil viscosity only [1].

3.5 Signal processing

The reflection coefficient is calculated experimentally by dividing the amplitude of the signal acquired from the solid-liquid interface by the amplitude of the signal obtained from a reference interface.

$$R = \frac{A_m}{A_r} \tag{12}$$

Where A_m is the amplitude of the reflected signal from the solid-oil contact interface and A_r is the reflected amplitude from the solid-reference interface. The reference medium is highly acoustically mismatched from the ultrasonic plug to guarantee maximum ultrasound reflectance. In this way, the

reflection coefficient calculated using equation (12) is a measure of how much the viscosity of the fluid influences the attenuation of the signal A_m. The air interface is commonly used as convenient reference in reflectance experiments. The main problem associated with the acquisition of the reflection coefficient in journal bearings is that there is no air interface that can be used as reference. This limitation is overcome by acquiring both the reference and the measurement signal together using a chirp signal.

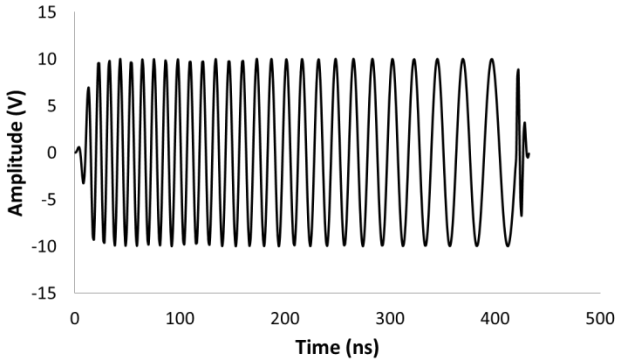

Figure 8: A chirp signal

A chirp (Figure 8) is a signal modulated in frequency that allows pulsing multiple frequencies with one burst. Using a chirp the portion of the signal that contains the resonance frequency component attenuates massively, while the portion of the signal with frequency component outside resonance does not attenuate. This means that part of the signal is very sensitive to the fluid and attenuates at the resonance frequency, and is equivalent to A_m, while the component outside resonance is not sensitive to the presence of the fluid, and is an ideal reference signal (A_r). Figure (9 a, b) shows schematically how this measurement method works.

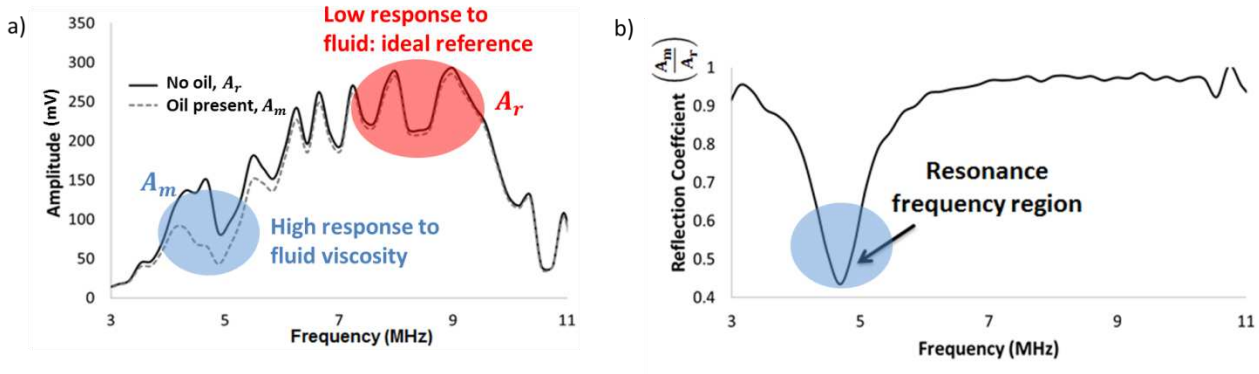

Figure 9: a) Amplitude spectra at a solid interface with and without oil. b) The reflection coefficient (equation 13) showing a resonance region sensitive to oil and a low response region when R is close to the unit value.

3.6 Procedure

The lubricant samples were tested at the rotational speed of 500 rpm and 1000 rpm and at different load levels. The rotational speeds and loads were chosen to simulate the temperature and pressure within the oil contact in conventional car engine journal bearings conditions. The rotational speed was chosen to simulate common values of journal rotational speed encountered in passenger car engines and the maximum rotational speed was limited by the motor inverter used for the

experiment. Different rotational speeds were chosen to obtain different temperatures at the contact and so detectable changes in viscosity due to the temperature rise. The loading conditions were chosen to obtain a maximum contact pressure of around 10 MPa (see also section 5). This value of pressure is in the expected magnitude order for passenger car journal bearings. Every experiment was repeated twice consecutively with a pause of one hour between every test run to disperse the heat accumulated during the previous experiment. Every time a new sample was tested the rig was cleaned by flushing the new test lubricant until only the new sample is present in the contact area. Table 2 reports the test matrix.

Sample	Load at 500 rpm (kN)	Load at 1000 rpm (kN)
Ester	12	12
PAO40	15	20
VM	12	15

Table 2: Experimental test matrix

3.7 Theoretical bearing model

The viscosity measured experimentally around the bearing circumference was compared with the well-known analytical solution from a semi-isoviscous model of the Reynolds equation for the hydrodynamic lubrication of journal bearings, using a finite differences algorithm [17]. A full thermo-elastohydrodynamic model of film formation and viscosity was beyond the scope of this work. Here a simplified approach was used to establish where the pressure variation in the bearing gap is such that the viscosity increases to a maximum. This value was then compared with the experimental results of the experimental data. Firstly the geometry of the bearing gap was obtained using the chart of Raimondi and Boyd [18]. The Raimondi-Boyd charts provide the solution for the Reynolds equation for one dimensional flow for different parameters (e.g., the film thickness). This solution is valid for the L/D ratio used in this research work. These charts were used to determine the eccentricity (ε) and the non-dimensional load W' for each oils for the two rotational speeds. Table 3 summarizes the input parameter of the semi-isoviscous model.

Parameter	Ester	PAO40	VM
$W'(1000\ \text{rpm})$	1.7109	0.9125	7.984
$W'(500\ \text{rpm})$	3.43	1.372	16
$\varepsilon\ (1000\ \text{rpm})$	0.425	0.29	0.72
$\varepsilon\ (500\ \text{rpm})$	0.58	0.39	0.82

Table 3: Entry parameters of the analytical model

For the purpose of this calculation, the oil viscosities were assumed to be constant and equal to the viscosity measured at the bearing mean operating temperature (also called effective temperature). Once the geometry of the bearing gap was determined a finite differences method was used to solve the Reynolds equation. The model assumed no elastic deformation, no shear heating, and, a constant viscosity. The output of the Reynolds finite difference method is the pressure distribution around the bearing. The pressure results from the model are shown in Section 4.3 and are used to calculate the angle at which the maximum load occurs as well as the expected maximum viscosity due to the pressure increment.

4. Results

4.1 Circumferential Viscosity Variation

Figures (10 a) shows an example of the viscosity results obtained along the bearing circumference for the PAO40 sample. In Figure (10 a) is possible to identify four different viscosity regions. These can be easily visualized in Figure (10 b) as a polar plot for the test conducted at 500 rpm. In this plot the temperatures reported in the different zones refer to the average temperatures measured by the thermocouple at the corresponding bearing position at the moment of data acquisition.

Zone 1 has low temperature and low load and is associated with the inlet region. The oil is fed at the angle of 30 degrees at room temperature and the viscosity value measured is equal to the viscosity of the oil at room temperature, η_0 in Table 2. This region is characterized by the lowest values of temperature and pressure.

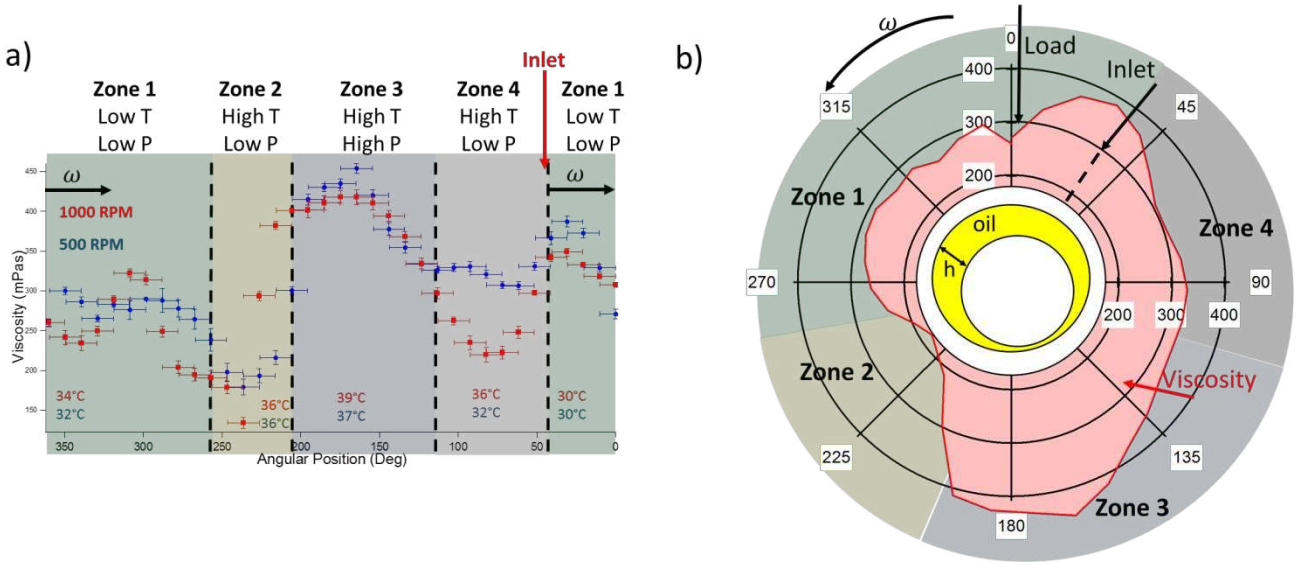

Figure 10: a) Angle-Viscosity plot for the PAO sample b) Bearing circumferential viscosity for the PAO sample

Zone 2 is characterized by high temperature and low load. This region is characterized by a drop in viscosity and it is also the area where minimum film thickness is expected. It is interesting to note that the viscosity profile in this region is similar to the one in zone 4. This is due to the fact that the temperature measured in zone 2 is very close to that measured in zone 4. In zone 2, therefore, the temperature effect is dominant since the load is not sufficient to increase the viscosity greatly.

Zone 3 is characterized by a temperature rise and high load. The viscosity measured in this zone is characterized by the superposition of the effects of temperature and pressure, as shown schematically in Figure (11). The film thickness shape in the upper figure is a function of the bearing profile, while in the middle sketch the viscosity is assumed to be a function of temperature only. The maximum temperature is usually coincident to the minimum film thickness or in the region immediately after the minimum film thickness: the higher the temperature, the lower the viscosity. Finally, the bottom sketch shows what happens when a pressure gradient is present. In this case, viscosity increases exponentially with the pressure thus explaining the viscosity curve shape.

In the zone 4, the temperature rises and the load is low. This zone is characterized by a lower value of viscosity because the temperature rises and the load value is negligible. It has to be noticed that the measured value of temperature is much higher than in zone 1 and there is a sudden drop as cold oil enters the bearing.

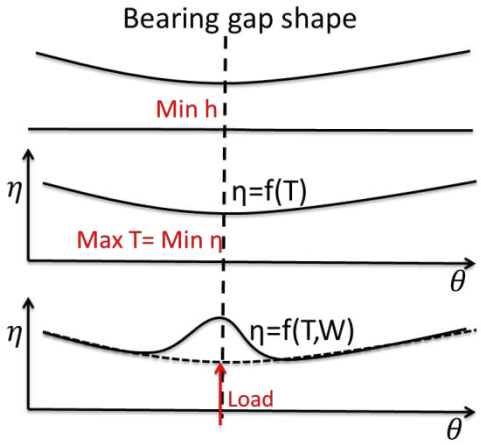

Figure 11: Schematic representation of the viscosity profile in the region under maximum load

4.2 Power Loss Variation

The viscosity results in conjunction with the calculated film thickness can be used to calculate the power losses at each position around the journal bearing circumference. Figure (12) shows the geometry of the bearing as an infinitesimal lubricant quantity is sheared at the contact interface. The power loss in this small element is given by:

$$d\dot{W} = \tau_x dA R\omega \tag{13}$$

Where $\tau_x dA$ is the shear force on the element of surface area *dA* and $R\omega$ represent the entraining velocity. This expression can be expanded in terms of the viscosity and shear rate $\dot{\gamma}$ as:

$$d\dot{W} = \eta\dot{\gamma} B dx R\omega \tag{14}$$

Where Bdx is the surface area. Assuming a linear velocity gradient then:

$$d\dot{W} = \eta \frac{R\omega}{h} B dx R\omega \tag{15}$$

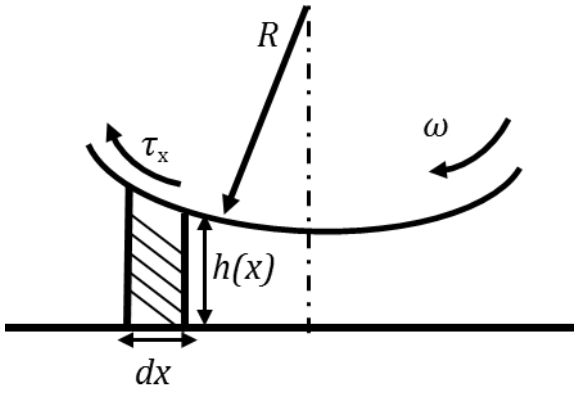

Figure 12: Scheme of the journal bearing geometry

Consequently:

$$\dot{W} = (R\omega)^2 B \int_0^L \frac{\eta}{h} dx \tag{16}$$

In section 4.1 the viscosity results were acquired at discrete locations. Then the integral in equation (16) is the sum of $\frac{\eta}{h}$ at each discrete location and dx becomes $\frac{2\pi R}{n}$ where *n* is the number of discrete points acquired. Therefore, equation (16) becomes:

$$\dot{W} = (R\omega)^2 B \sum_{i=1}^{n} \frac{\eta_i}{h_i} \frac{2\pi R}{n} \tag{17}$$

The film thickness is calculated using the Raimondi-Boyd [19] charts with the input parameters provided in section 4.1 in Table (3) as:

$$h_i = c(1 + \varepsilon cos\theta_i) \tag{18}$$

Figure (13 a, b) shows the power loss for each discrete region. These are calculated using (17) and the viscosity results for Figure (16). Figure (13 c, d) shows the total power losses obtained cumulatively at each location using equation (17). The total power losses are compared with the Petroff [17] equation for the approximated total power losses in a plain journal bearing:

$$\dot{W}_P = \frac{2\pi^2 \eta B R^2 W \omega}{9549 Pc} \tag{19}$$

Where $\dot{W}_P$ is the Petroff total power loss in a plain journal bearing.

The majority of the power loss occurs in the maximum loaded region where the higher viscosity and minimum film thickness are present. Figure (14) shows, as an example, on a polar graph the power losses versus angle for the Ester oil at 500 rpm. The graph shows that the majority of the power losses are concentrated in the small area where the film thickness is minimum and the pressure is maximum.

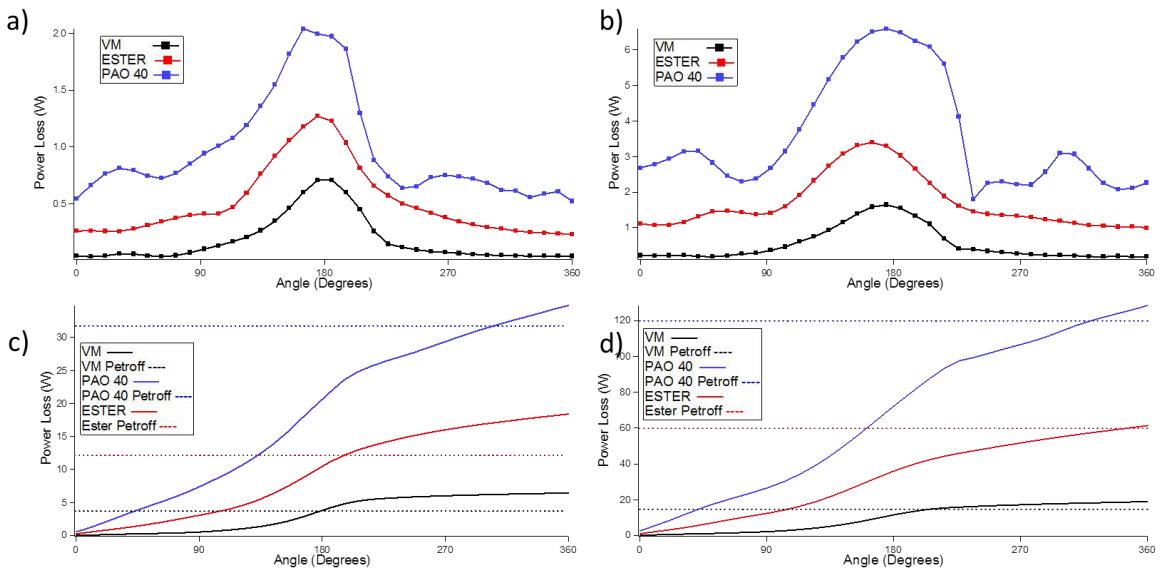

Figure 13: Power loss distribution around the journal bearing circumference for two rotational speeds: a) local power loss at 500 rpm, b) local power loss at 1000 rpm, c) cumulative power loss at 500 rpm, d) cumulative power loss at 1000 rpm

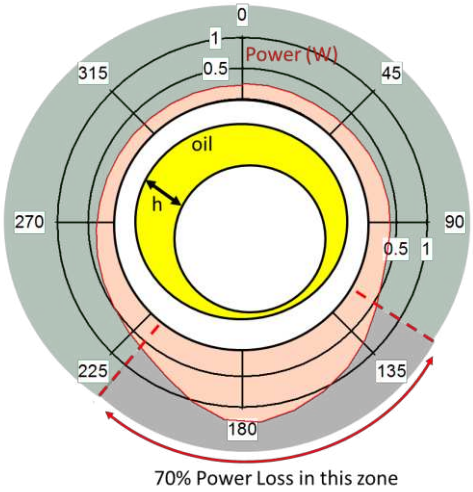

Figure 14: Power loss (W) in the journal bearing for the Ester sample. Over 70 % of the total losses happen in the region where the viscosity is higher

4.3 Results comparison with a semi-isoviscous model

The experimental angle-viscosity results were compared with the finite element semi-isoviscous solution of the Reynolds equation. This model calculates the pressure distribution around the journal bearing, given the input parameters reported in Table (3), Section 3.7. Figure (15) shows the pressure field obtained as solution of this model.

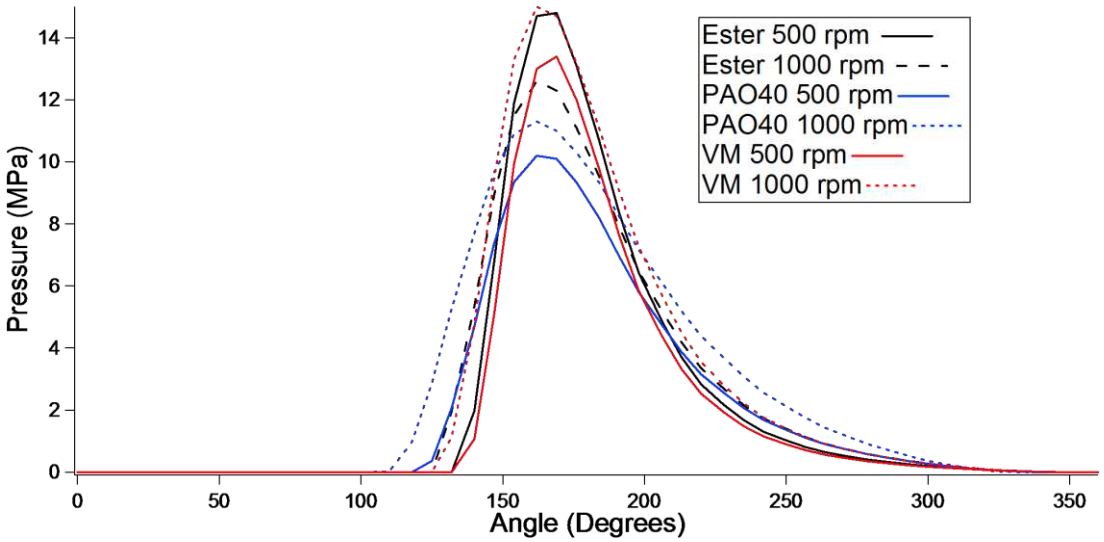

Figure 15: Pressure field in the journal bearing for the different oils at the different testing conditions

The pressure field of Figure (15) was then used to predict the viscosity change in the oil according to the Barus equation:

$$\eta = \eta_0 e^{\alpha p} \tag{20}$$

Where η is the viscosity at pressure p and η_0 is the viscosity at atmospheric pressure. A more complete model would use this viscosity variation to iterate a new gap shape and pressure profile. For simplicity this was not done in this work.

Figure (16) shows the comparison of the viscosity-angle results for the ultrasonic viscometer and the semi-isoviscous model. The ultrasonic viscometer identifies clearly the region at which maximum pressure occurs and where the viscosity increases. The semi-isoviscous model does not calculate the variation of viscosity with the temperature variation. The shape of the experimental ultrasonic viscometer curves is characterized by the influence of thermal effects, contrary to the semi-isoviscous curve. Outside the loaded region, where the temperature is varying, but the load is not, there is no change in viscosity and the model and experimental curve differ substantially. The shape of the experimental curve is influenced by both pressure and temperature effects.

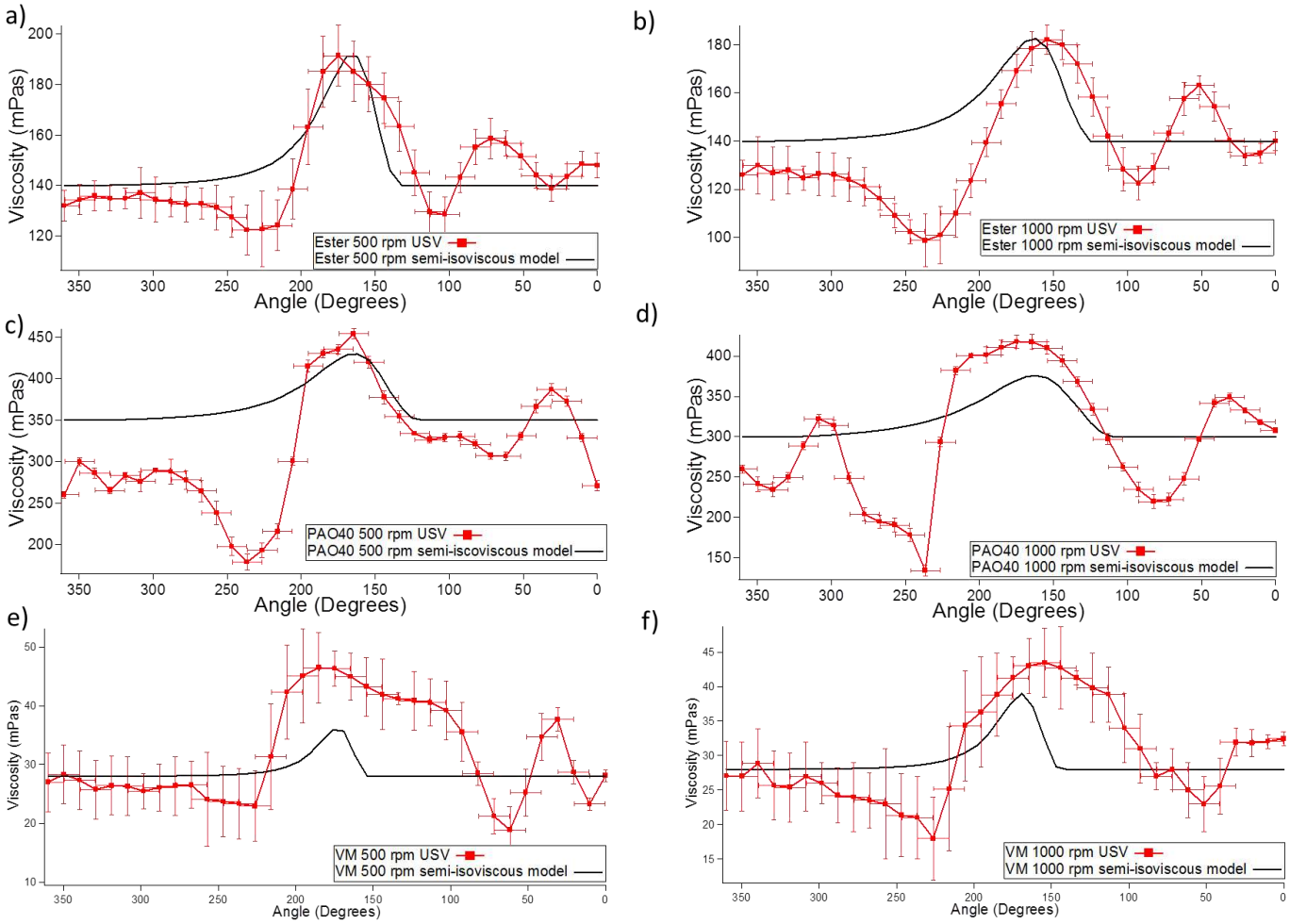

Figure 16: The circumferential viscosity profile in a journal bearing. Comparison between semi-isoviscous model and ultrasonic matching layer viscometer

6. Conclusions

This paper illustrates the application of an ultrasonic matching layer method to measure viscosity in-situ in an operating journal bearing. The ultrasonic viscometer was mounted in the journal to allow measurement of the circumferential viscosity at different rotational speeds and loads. The results show four different viscosity regions: low temperature and low load, high temperature and no load, maximum load and temperature, high temperature and no load. These regions are consistent with the viscosity field expected by superposition of the effects of the temperature and pressure gradient that were measured. The importance of the viscosity results is enhanced by quantifying the power losses in the bearing. It is shown that the majority of the losses are localized in the small area where the film thickness is minimum and the load is maximum. The experimental results were compared with a simulation of the Reynolds equation for journal bearings hydrodynamic lubrication. The comparison of the results shows that the ultrasonic viscometer and the model identify the same loaded region and the same angle at which the maximum load occurs. The discrepancies between the maximum viscosity measured with the numerical model and the viscometer is due to the fact that the numerical model does not take into account thermal effects and shear heating. The findings

of this research have significant impact in the automotive and lubricant industries It significantly advances the understanding of the complex lubrication conditions found in engine contacts and further validates the existing lubrication models. The scientific experimental techniques and fundamental knowledge generated by this research aid the design of advanced lubricant formulations.

References

1. Schirru, M., Mills, R., Dwyer-Joyce, R., Smith, O., and Sutton, M. (2015). Viscosity Measurement in a Lubricant Film Using an Ultrasonically Resonating Matching Layer. *Tribology Letters*, *60*(3) pp. 1-11.
2. Mason, W.P., Baker W.O., McSkimin, H.J. et al. (1948). Measurement of shear elasticity and viscosity of liquids at ultrasonic frequencies. *Physical Review.* Vol. 75(6) pp. 936-946
3. Bujard, M.R., (1989) Method of measuring the dynamic viscosity of a viscous fluid utilizing acoustic transducer. *US Patent Number 04862384*
4. Emmert, S.W., (1986) Apparatus and method for determining the viscosity of a fluid sample. *US Patent Number 4721874*
5. Greenwood, M.S,. and Bamberger, J.A., (2002) Measurement of viscosity and shear wave velocity of a liquid or slurry for on-line process control*. Ultrasonics* Vol. 39 pp. 623-630
6. Lamb, J., (1967) Physical properties of fluid lubricants: rheological and viscoelastic behaviour. *Proceedings of the Institution of Mechanical Engineers, Conference Proceedings.* Vol. 182 pp. 293-310
7. Barlow, A.J., and Lamb, J., (1959) The visco-elastic behaviour of lubricating oils under cyclic shearing stress. *Proc. R. Soc. Lond*. Vol 253 pp. 52-69
8. Dowson, D. G. R. A. V., Higginson, G. R., and Whitaker, A. V., (1962) "Elasto-hydrodynamic lubrication: a survey of isothermal solutions." Journal of Mechanical Engineering Science 4.2 pp. 121-126.
9. Schirru, M., and Dwyer-Joyce, R.S., (2015) A model for the reflection of shear ultrasonic waves at a thin liquid film and its application to viscometry in journal bearings. *Proc IMechE Part J: J Engineering Tribology*, [online] accessible from: http://pij.sagepub.com/
10. Collin, R.E., (1955) Theory and design of wide-band multisection quarter-wave transformers. *Proceedings of the IRE* Vol.36 pp. 621-629
11. Emmert, S.W., (1986) Apparatus and method for determining the viscosity of a fluid sample. *US Patent Number 4721874*
12. Bair, S., and Winer, W.O., (1980) Some observations on the relationship between lubricant mechanical and dielectric transitions under pressure, *Trans. ASME, Journal of Lubrication Tech*., 102, 2, pp. 229-235
13. Hutton, J.F., (1967) Viscoelastic relaxation spectra of lubricating oils and their component fractions. *Proc. Roy. Soc. London Mathematical and Physical Sciences.* Vol. 304, 1476, pp.65-80
14. Johnson, K. L., & Tevaarwerk, J. L. (1977). Shear behaviour of elastohydrodynamic oil films. *Proceedings of the Royal Society of London A: Mathematical, Physical and Engineering Sciences* Vol. 356, No. 1685, pp. 215-236
15. Kinsler, E., et al. (2000) *Fundamentals of acoustics* , 4th Edition, Wiley, New York

16. Harrison, G., and Barlow, A.J.,. (1981) Dynamic Viscosity Measurement. *Methods of experimental physics* 19 pp. 137-178.
17. Stachowiack, G.W., and Batchelor, A.W., (2001) *Engineering Tribology.* 2nd ed. Butterworth Heinemann
18. Raimondi, A.A., and Boyd, J., (1958) A solution for the finite journal bearing and its application to analysis and design. *ASLE Transactions*. Vol. 1 pp. 159-209
19. Juvinall, R.C., and Kurt, M.M., (2006) *Fundamentals of machine component design*. 5th ed., John Wiley & Sons